

# The Late Paleozoic fold–thrust structure of the Tunka bald mountains, East Sayan (*southern framing of the Siberian Platform*)

A.B. Ryabinin<sup>†</sup>, M.M. Buslov<sup>\*</sup>, F.I. Zhimulev, A.V. Travin

*V.S. Sobolev Institute of Geology and Mineralogy, Siberian Branch of the Russian Academy of Sciences,  
pr. Akademika Koptyuga 3, Novosibirsk, 630090, Russia*

Received 11 April 2011; accepted 31 May 2011

Available online xx November 2011

## Abstract

According to the new geological, geochronological, and structural data, the Tunka bald mountains (East Sayan) have a nappe structure, which formed in the Late Carboniferous–Early Permian. The deformations have been dated by the  $^{40}\text{Ar}$ – $^{39}\text{Ar}$  method on the basis of syntectonic micas and amphiboles, whose structural and spatial positions have been determined in oriented thin sections. The geometrical analysis of macro- and microstructures has revealed three development stages of the structures, which followed one another in progressive deformation. The first (thrust-fault) stage (316–310 Ma) comprised a group of N-verging thrust sheets. In the second (fold deformation) stage (305–303 Ma), they were folded. The third (strike-slip fault) stage (286 Ma) comprised high-angle shears, along which V-shaped blocks were squeezed westward from the most compressed areas. All the structures developed under near-N–S-trending compression. The thrusting in the Tunka bald mountains was coeval with the major shear structures in the eastern Central Asian Fold Belt (Main Sayan Fault; Kurai, Northeastern, and Irtysh crumpled zones, etc.). Also, it was simultaneous with the formation of continental-margin calc-alkalic and shoshonite series (305–278 Ma) as well as that of the alkali and alkali-feldspar syenites and granites (281–278 Ma) of the Tarim mantle plume in the Angara–Vitim pluton, located near and east of the studied region. Thus, the simultaneous development of the Late Paleozoic structures, active-margin structures, and plume magmatism in southern Siberia might have resulted from the global geodynamic events caused by the interaction between the tectonic plates which formed the Central Asian Fold Belt.

© 2011, V.S. Sobolev IGM, Siberian Branch of the RAS. Published by Elsevier B.V. All rights reserved.

**Keywords:** Late Paleozoic folding, thrusting, and shearing; microstructural analysis; dynamic analysis; Main Sayan Fault; East Sayan; Siberian Platform

## Introduction

In the last few decades, an Early Paleozoic nappe structure (Boos, 1991; Dobretsov, 1985, 1988) and the igneous and metamorphic complexes (Donskaya et al., 2000; Gladkochub et al., 2010; Kotov et al., 1997; Reznitskii et al., 2007; Rytsk et al., 2000; Turkina et al., 2007) making up the Cisbaikalia collisional belt have been distinguished and described in the southwestern folded framing of the Siberian craton (East Sayan and Cisbaikalia). Most of the dates for the rock complexes of the Cisbaikalia metamorphic collisional belt are within a range of 500–470 Ma. It has been shown that the nappe structure of the East Sayan, including its southeastern part, which is distinguished as the Tunka terrane (Belichenko et al., 2003) or the Il'chir zone (Fedotova and Khain, 2002),

formed in the Ordovician owing to the accretion of the Tuva–Mongolian microcontinent (TMM) to the Siberian craton (Belichenko et al., 1994, 2003). In the west of the Tunka bald mountains, the upper boundary of the Early Paleozoic stage of deformations and metamorphism is determined by the suture granites of the Munku-Sardyk pluton. The intrusive contact of the pluton cuts metamorphic zoning, suggesting that the granites are postmetamorphic (Reznitskii et al., 2007). The U–Pb age of the granites is  $481 \pm 2$  Ma, and the Sm–Nd model age is 1.8 Ga; this suggests the participation of the ancient continental crust, probably belonging to the TMM, in the melting. The dating of high-grade complexes and postmetamorphic intrusions in the Sayan–Baikal Fold Region suggests that Early Paleozoic accretionary–collisional complexes are widespread in the region (Dobretsov and Buslov, 2007).

Also, during a medium-scale geological survey in the southeastern Tunka bald mountains (Fig. 1), nappe outliers were found; they consisted of metamorphic rocks and overlay the red-colored conglomerates and sandstones of the Sagan-Sair Formation, regarded as orogenic molasse (Butov et al.,

<sup>†</sup> Deceased.

<sup>\*</sup> Corresponding author.

*E-mail address:* [misha@igm.nsc.ru](mailto:misha@igm.nsc.ru) (M.M. Buslov)

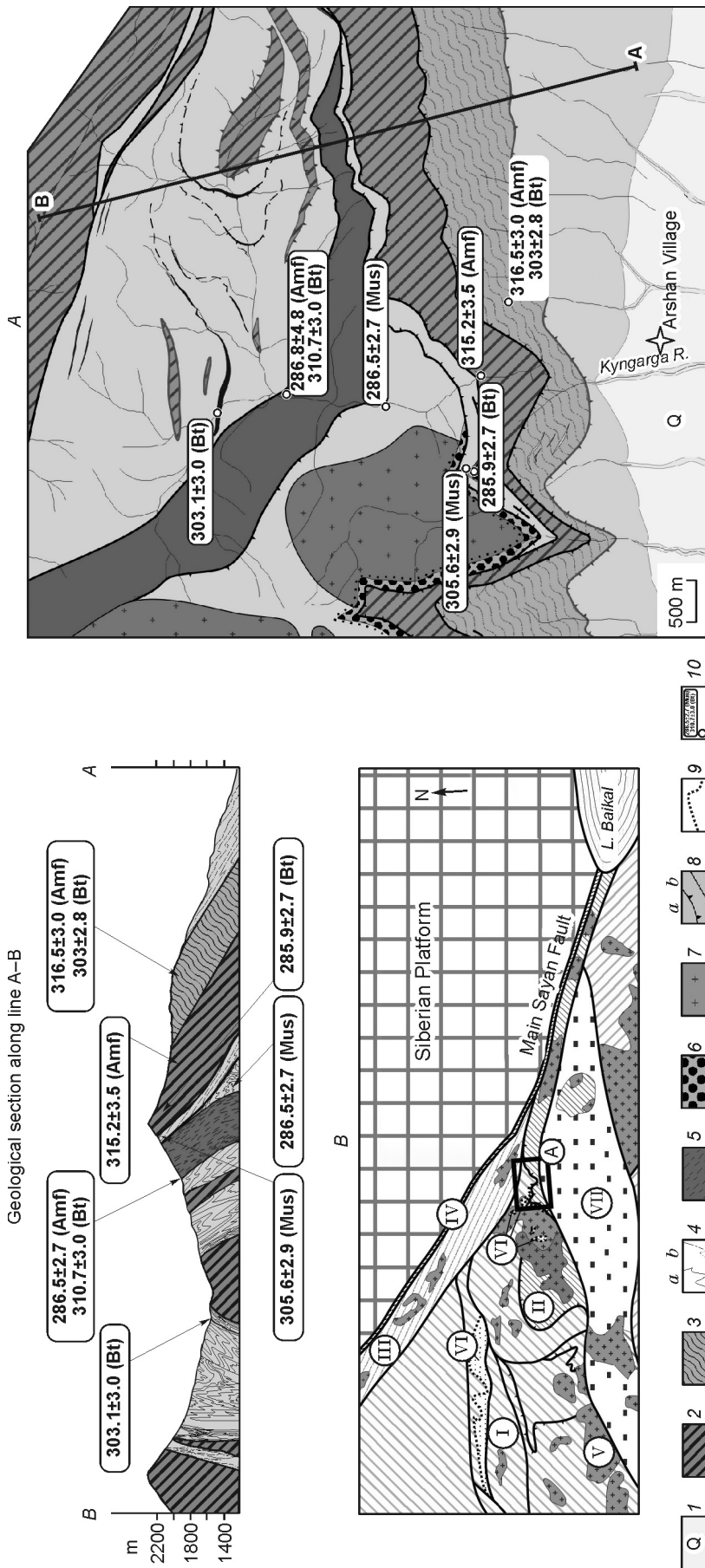


Fig. 1. Geologic structure of the Arshan area (A) and its location in the southern framing of the Siberian Platform (B). A, 1, Quaternary sediments; 2, gneisses, mafic granulites, garnet amphibolites; 3, mélangé zone with diaphorized plagiogneisses, mafic granulites, garnet amphibolites, and mylonitized marbles; 4, mylonitized marbles; 5, gneisses, mafic granulites, garnet amphibolites, actual (a) and presumed (b); 6, Late Devonian–Early Carboniferous molasse (Sagan-Sair Formation); 7, Late Devonian microcline granites and granosyenites; 8, ruptures with inclined (a) and steep (b) fault planes; 9, stratigraphic contact; 10, sampling sites and results of Ar–Ar dating. B, I, II, Deformational complexes: I, Early Paleozoic; II, Late Paleozoic; III, Late Paleozoic Kitoi-Kin deformational zone; IV, Main Sayan Fault; V, Late Paleozoic granitoids; VI, Late Paleozoic molasse; VII, Cenozoic Tunka basin.

2001). The formation was dated at the Permian on the basis of numerous fish scales, plant impressions, spores, and pollen (Butov et al., 2001). The sediments of the Sagan-Sair Formation overlie the eroded surface of the microcline granites of the Sayan (Sarkhoi, or Zun-Muren (Vilor et al., 1991)) complex. The granite plutons of the Sayan complex seal the folded structure formed by the tectonic sheets of the Upper Shumak metaterigenous and Gorlyk carbonate formations. These formations are assigned to the sedimentary cover of the TMM (Letnikova and Geletii, 2005) and dated at the Vendian–Early Cambrian (Anisimova et al., 2010; Letnikova and Geletii, 2005). Thus, before the accumulation of the Sagan-Sair Formation, a nappe structure comprising the Gorlyk and Upper Shumak Formations had formed; this was followed by the emplacement of the granites of the Sayan complex. Afterward the upper part of this structure was eroded and the sealing granite plutons were exposed. The sediments of the Sagan-Sair Formation in the region form asymmetric V-shaped basins, partly overlain by N-verging thrusts (for example, the Sagan-Sair syncline). These relations are evidence for two thrusting stages in the Tunka bald mountains: before and after the accumulation of the Sagan-Sair Formation.

Some igneous and metamorphic complexes of the Tunka terrane are Late Paleozoic. The metamorphic rocks from the Arshan area were dated at 316–286 Ma (Buslov et al., 2009). The syntectonic metasomatic rocks of the Main Sayan Fault (MSF), which separates the Sharyzhalgai salient of the Siberian craton from the Altai–Sayan Fold Region (Fig. 1), are Late Carboniferous (321–309 Ma (Savel'eva et al., 2003)). The MSF contains several generations of granite veins, the oldest being Early Carboniferous ( $353 \pm 1.9$  Ma, U–Pb dating) and the youngest Early Permian ( $278.2 \pm 4.3$  Ma, U–Pb dating) (Savel'eva et al., 2006, 2010). Late Carboniferous ( $312 \pm 20$  Ma (Belichenko et al., 1988)) zonal metamorphism is observed in the central Tunka terrane.

A close age was yielded by the granites of the Angara–Vitim pluton (Tsygankov et al., 2007, 2010), which features continental-margin calc-alkalic and shoshonitic granitoids (305–278 Ma) as well as the alkali and alkali-feldspar syenites and granites (281–278 Ma), which belong to the giant igneous province of the Tarim plume (Borisenko et al., 2006; Dobretsov et al., 2010).

The observed structure of the fold region results from at least two large orogenic stages: Early Paleozoic (Late Cambrian–Middle Ordovician) and Late Paleozoic (Late Carboniferous–Permian). The Late Paleozoic stage in the development of the region structure is coeval with large-scale strike-slip tectonics in the western Altai–Sayan Fold Region (Buslov, 2011; Buslov et al., 2003) and granitic magmatism (Tsygankov et al., 2007) and metamorphism (Mazukabzov et al., 2010) in western Transbaikalia. The Ordovician events in the region are well-studied and attributed to the accretion of the TMM and other terranes to the Siberian craton, whereas the scale of the Late Paleozoic structures, as well as their formation stages, age, and conditions, are poorly studied.

Our work is aimed at describing the Late Paleozoic nappe and shear structures of the Tunka bald mountains, refining

their age, and determining their scale and causes. It will contribute to studies of the structural evolution of the Sayan–Baikal segment of the Central Asian Fold Belt. The Tunka bald mountains (East Sayan) have a complex nappe structure, dominated by variously metamorphosed Early Paleozoic terrigenous, volcanic, and carbonate rocks (Boos, 1991). The present structure is a tectonic combination of the low-grade complexes of the TMM cover and high-grade counterparts of the Slyudyanka and Khangarul (Khamar-Daban) Groups. Retrograde dynamic metamorphism of the epidote–amphibolite and greenschist facies is observed in rupture zones.

During the 2006–2009 field trips, the Arshan area in the Tunka bald mountains, occupying the Kyngarga, Kharimta, Arkhut, and Belokopytka River basins, was studied in detail. During mapping, the structural forms of metamorphic rocks (fold-bend orientation, mineral and aggregate banding and linearity) were studied and oriented metamorphic-rock samples were taken for microstructural analysis and Ar–Ar dating. The internal structure of the tectonic sheets and dynamically metamorphosed rocks along their contacts was studied in detail to determine the kinematic and dynamic conditions needed for the formation of the nappe structures in the eastern Tunka bald mountains. The macro- and microstructural analyses and kinematic data were used to determine the orientation of the final strain ellipsoid and, correspondingly, the principal normal stresses when the structure was completely formed.

### Technique for the structural analysis of complexly dislocated complexes

The structural and compositional complexes in the eastern Tunka bald mountains are a typical example of complexly dislocated metamorphic rocks which formed in several stages of deformation and metamorphism. Under these conditions the possibilities of traditional techniques of geological mapping (crossing, tracing, and others) are limited by the abundance of ruptures, the absence of reliable stratigraphic boundaries, the disappearance of primary structures during metamorphism, the inconsistency of beds, units, and other geologic marker bodies along strike, and intense folding. Therefore, geometrical, kinematic, and dynamic analyses, based on macro- and microstructural data, were used for studying the morphology, orientation, and conditions needed for the formation of the folded structures in the area. The structural and geological methods used in our study are described in detail in special guides and monographs (Lukin et al., 1965; Mel'nikov et al., 2001; Passchier and Trouw, 1996; Rodygin, 2001; Saranchina, 1963; Turner and Weiss, 1963; Twiss and Moores, 1992).

**Geometrical analysis** on a stereographic projection is the most widely used technique for processing structural data. We used an equiangular stereographic projection (Wulff net) to the upper hemisphere. Geometrical analysis of macrostructure revealed areas with different folding parameters (folded-structure domains). Analysis of spatial data on the stereographic projection made possible a quantitative description of struc-

tures in a given area (for example, general folding parameters, the presence of cylindrical or conic shapes).

Kinematic and dynamic analyses of various-scale structures were used to determine the conditions needed for the formation of the complexly dislocated nappe complexes in the study region. **Kinematic analysis** presupposes restoring the direction of relative movements during the deformation without regard to their driving forces. Attempts at solving this problem only with the help of macrostructural data in heavily deformed complexes do not always have satisfactory results. In this case, to determine the shift sign, the macrostructural data should be combined with the microstructural ones, obtained from the study of oriented thin sections. Note that the subject of special analysis is the internal structure of syntectonic porphyroblasts: “snowball” structures, trains of recrystallized matter around porphyroclasts, partly shifted porphyroclasts, “pressure shadows,” mica fish, rolling structures, etc. The shift sign should be determined in the section parallel to linearity (especially that of minerals) regardless of the rotational axis, because linearity reflects the deformation direction in the rocks.

**Dynamic analysis** presupposes restoring the orientation of forces and the principal normal stresses, which cause deformation. The deformation on the scale of the studied objects was assumed to be homogeneous. In all the studies, the angle between the compression axis and shear planes (planes of maximum shear stresses) was taken to be  $45^\circ$ . Since the studied rocks originally had anisotropy (generally, the angle between the compression axis and shear planes is not strictly  $45^\circ$ ), we can speak about compression–extension zones when analyzing the results; this implies that the planes of maximum shear stresses occupy a somewhat uncertain position. This determines the error of the method.

**Microstructural analysis** is, first and foremost, a technique for studying rocks which helps to reveal mineral orientation. Under dynamic crystallization the orientation of some rock-forming minerals gives the most reliable insight into the conditions needed for the rock deformation. A correct observation of these microstructures is possible in sections perpendicular to the rotational axis. Correspondingly, the sampling should be perpendicular to schistosity (mylonite planarity) and parallel to the  $a$ -linearity of the rock (Rodygin, 2001). As a rule, the thin section should be perpendicular to rotational axis  $b$  (that is, lie on plane  $ac$ ).

We studied the crystallographic and crystalloptical elements of the minerals making up the rock: cleavage, jointing, translational twins, and bending/fracture structures, which showed a regular distribution. During the deformation individual grains make differential movements in the rocks with respect to one another or are deformed along sliding or twinning planes, that is, along certain lattice planes with the maximum reticular density. The integral result of these movements is general rock deformation. All the measurements were taken in oriented thin sections with the help of a Fedorov theodolitic stage (Saranchina, 1963).

As regards the foliated minerals, the tectonic orientation of muscovite, biotite, and chlorites is best studied. The perfect cleavage of these minerals along basal plane  $c(001)$  is parallel

to the differential-sliding planes in the rock (in the case of a simple strike-slip fault). Mica crystals forming under simple strike-slip faulting are predominantly oriented so that cleavage plane  $c(001)$  coincides with the planes of maximum shear stresses in the growth region. The studied rocks contain quite a number of crystals with undulation and cleavage bends and fractures, resulting from the deformation of previously formed crystals. The king-bands, as a rule, have a regular orientation, which coincides with axis  $b$ . Thus, while measuring the orientation of foliated minerals, we can record the shear stress orientation at the “mineral–rock” level by the moment of microstructure formation and speak about the mechanisms of deformation and the accompanying movements.

Studies of deformed carbonate rocks and experiments on the deformation of carbonate single crystals revealed the deformational origin of polysynthetic twins, which result from sliding along variously directed planes. The most frequent translation-gliding plane in calcite grains is plane  $e(01\bar{1}2)$ ; in dolomite grains, plane  $f(02\bar{2}1)$  (Fig. 2). The mechanical twinning of calcite grains occurs along plane  $e(01\bar{1}2)$  only by sliding toward the short diagonal of the cleavage rhombohedron (parallel to the crystal optic axis). Calcite has three such planes, which are mechanically equal. As a rule, translation gliding occurs along one plane (more rarely, along two planes) at a time. For the dynamic analysis in this work, we studied massive marbles, carbonate mylonites, and quartz–carbonate mylonites in oriented thin sections using a Fedorov theodolitic stage. We determined the orientation of translational twins

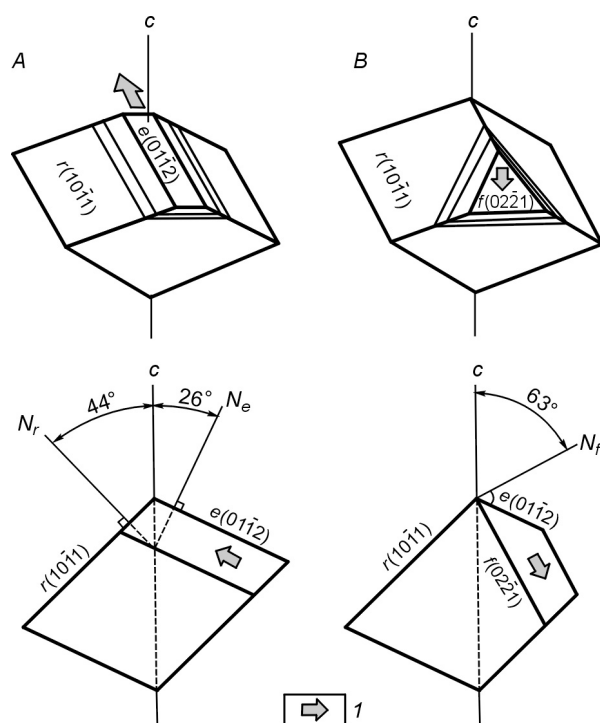


Fig. 2. Orientation of the main crystallographic planes and the directions of twin sliding, with angle ratios between them (1) in calcite (A) and dolomite (B) crystals. Ne, Nr, Nf, Normals to planes  $e(01\bar{1}2)$ ,  $r(10\bar{1}1)$ , and  $f(02\bar{2}1)$ , respectively (Saranchina, 1963).

(faces  $e(01\bar{1}2)$  of an obtuse rhombohedron along which differential sliding takes place and, correspondingly, the shear stresses and fracture bends of twins resulting from progressive deformation are realized). The middle position of the twin fracture bends, as a rule, coincides with axis  $b$ . The case when the sliding occurred almost simultaneously along two planes was an exception: we observed variations in the orientations of the fracture bends of the twins, which lay approximately on plane  $cb$ . The relationships considered belong to the cases of single-stage deformation. Staged deformation is often reflected in the presence of variously aged twins, which might cross or displace one another. Sometimes several directions of twinning planes are identified; consequently, the deformation has its peculiar features in different structuring stages.

Deformation in amphibolites was studied by the technique for studying the orientation of amphibole. The cleavage of green hornblende  $\{110\}$  and its jointing across the elongation  $\{001\}$  were measured.

Using microstructural kinematic indicators together with macrostructural ones permits determining the orientation of the axis of the final strain ellipsoid for the rock and restoring the orientation of the forces and the principal normal stresses causing the deformation.

### Geologic structure of the Arshan area

During the mapping the structural forms of metamorphic rocks were studied (fold-bend orientation, mineral and aggregate banding and linearity). Oriented samples of metamorphic rocks were taken for microstructural analysis and Ar–Ar dating. Structural data on the outcrops were grouped depending on lithology and the orientation of directional structures. Similar structural characteristics of the outcrop groups, in turn, permitted distinguishing several domains. The area (from north to south) is divided into several structural–compositional domains (Fig. 3). We studied in detail the South and North Arshan domains and the Arkhut–Kynygarga fault, which feature the completest range of Late Paleozoic structures.

### South Arshan domain

The domain consists of lithologically different metamorphic rocks: calcitic; calcite–muscovite; calcite; phlogopite; diopside marbles; carbonaceous–carbonate mylonites; metaterigenous greenschists; monomineralic, plagioclase, and plagioclase–biotite amphibolites and mafic granulites; biotitic plagiogneisses (Fig. 4).

The domain can be divided into some tectonic sheets differing in their lithology and separated by rupture zones. Their boundaries feature schistose and undulose zones with newly formed foliated minerals (micas, chlorites). In the north of the domain, the tectonic sheets are overthrust upon the unmetamorphosed sediments of the Sagan-Sair Formation (red-colored sandstones and fine-clastic conglomerates). On the watershed of the Rivers Zun-Khandagai and Tolta,

Bugatai, Bukhota, and Kynygarga, the Sagan-Sair Formation consists of polymictic conglomerates, gravelstones, and red-colored sandstones interbedded with cherry-red siltstones (Fig. 5, *a*). The conglomerates overlie the eroded marble surface with a well-defined structural unconformity (Fig. 5, *c, d*) and dip gently southward at 5–10°. The Sagan-Sair Formation is overlain, with a tectonic contact, by undulose chloritized gneisses, making up several tectonic outliers, which are distinct in the topography (Fig. 5, *c, e, f*). The tectonic contact is usually overlain by loose slope sediments, and the near-contact changes in the sedimentary rocks are probably manifested only in a discontinuity. The rocks are neither deformed nor metamorphosed, suggesting that the nappes formed near the surface. The Sagan-Sair Formation in the study area is 40–50 m thick. On the watershed of the Bukhota, Bugatai, and Kynygarga Rivers, it is dominated by polymictic conglomerates with thin interbeds of poorly sorted red-colored coarse sandstones (Figs. 1; 5, *b*). They overlie the eroded surface of microcline granites with a southward dip (azimuth 150  $\angle$  25°) and are overlain (with a tectonic contact) by schistose chloritized gneisses. Their thickness reaches 100 m. Near the contact with the gneisses, there is a thin (up to 1 m) zone of the mylonitized rocks of the Sagan-Sair Formation. Lower down the section, no deformation or metamorphism are observed. Note that the dip angle of bedding in the sedimentary rocks of the Sagan-Sair Formation (like that of the fault plane for the nappes) increases from west to east, suggesting that the tectonic sheets and underlying sediments were deformed later.

The sheets have a complex folded structure. Two fold generations are distinguished:  $F_1$  (with kinematic layer-by-layer flow, Fig. 6) and  $F_2$  (viscoplastic-fracture and bending folds, depending on lithology and position in the structural contour). The  $F_1$  folds have complex disharmonious structures, often with detached curves. Schistosity (parallel to the limbs of the recumbent  $F_1$  folds) predominates in the compositionally different rocks. In the amphibolites it is due to the amphibole orientation; in the marbles and calciphyres, to the orientation of calcite and mica (paragonite, muscovite, phlogopite).

The fold bends dip southwestward at ~20°. The  $F_1$  folds are cylindrical. Note that stereograms most often show not the fold bend along the great-circle arc but only one maximum, corresponding to the outcrops of the fold-limb normals and  $S_1$  schistosity, which is parallel to them (Fig. 6).

Depending on the position of the deformed rocks in the sheet complex, the  $F_2$  folded structures have different morphology. The formation of these folds accompanies retrograde greenschist metamorphism (up to the sericite subzone). Note that viscous-fracture folds develop in chlorite–sericite diaphthorites after plagioclase amphibolites. Analysis of movements along synfolding ruptures in the South Arshan domain shows that the kinematics remained unchanged during the formation of  $F_1$  and  $F_2$  folded structures.

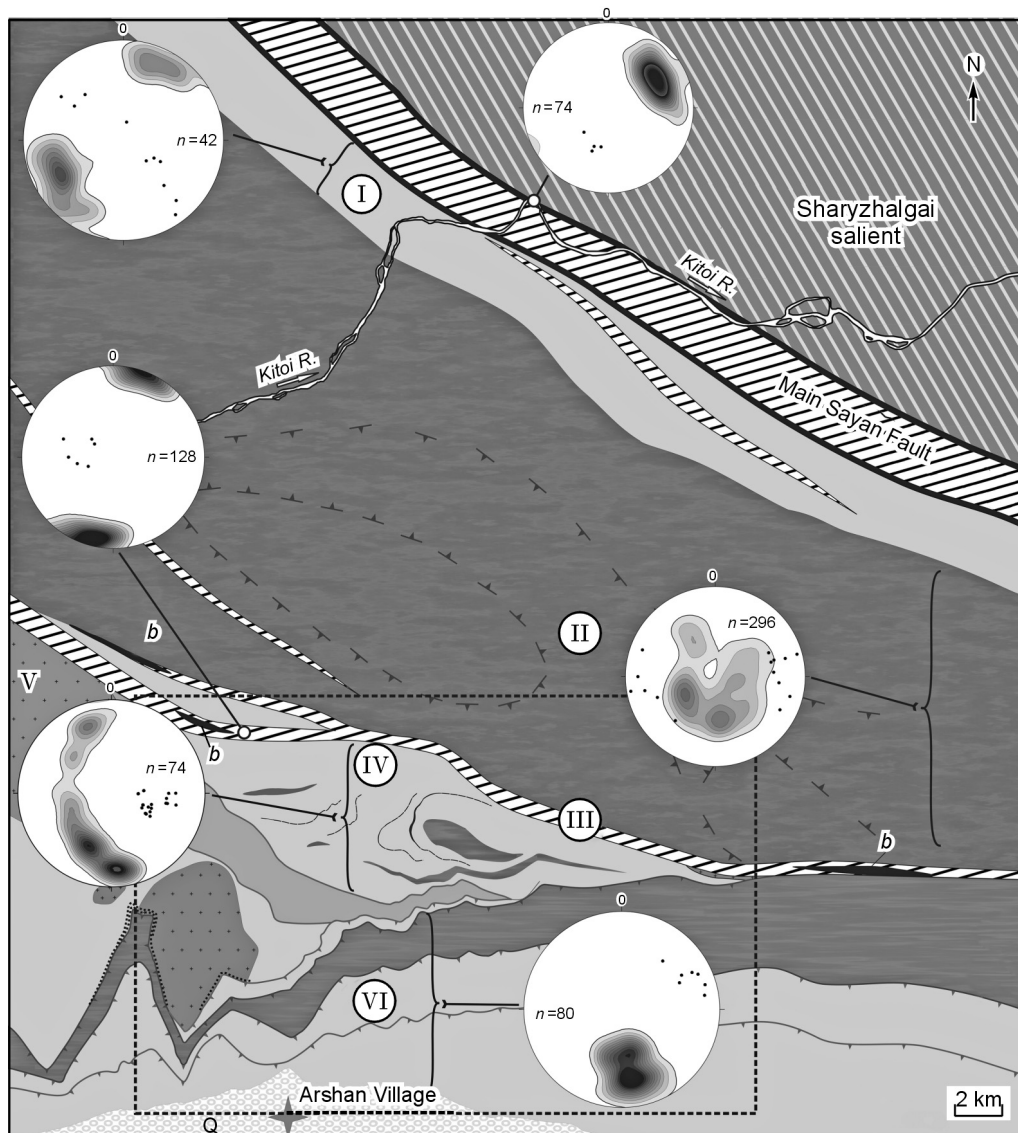


Fig. 3. Structural and geological sketch map of the eastern Tunka bald mountains. Structural–compositional domains: I, Kitoi (Main Sayan Fault); II, Belokopytka (marbles, calciphyres, quartz–carbonate mylonites, carbonaceous–carbonate mylonites); III, Arkhut (amphibolites, garnet amphibolites, cut subconformably by gneissose tonalites–granodiorites); IV, Arkhut–Kynrgarga fault; V, North Arshan (marbles, garnet–mica schists, subconformable bodies of amphibolites and biotitic gneisses); VI, South Arshan (amphibolites, marbles, and calciphyres, cut by plagiogranites–granodiorites). On the stereograms isolines show the schistosity bedding (increment 1%) and dots show the orientation of the bends of the synchronous folds. Rectangle marks the boundaries of the well-studied Arshan reference locality.

### Microstructural analysis of the metamorphic rocks from the South Arshan domain

The study presents the results of microstructural analysis for the rock samples from the southern sheet (marbles), and from the northern one (amphibolites, gneisses) (Fig. 4). The geologic structure of the marble sheet was studied in the Kynrgarga and Kharimta River canyons. In sample T09003 of diopside marble (Cal, Di, Phlog, Qtz), the orientation of translational twins (face  $e$  of an obtuse rhombohedron along which differential sliding takes place and, correspondingly, the shear stresses are realized) and the fracture bends of twins resulting from progressive deformation were determined in a thin section. An oriented sample was taken perpendicular to  $S_1$  schistosity. On the stereogram (Fig. 7,  $a$ ), the normals to

the twinning planes formed an area with a maximum corresponding to the main shearing surface (dip azimuth  $184 \angle 49^\circ$ ). The twin fracture bends formed a distinct maximum ( $b_2$ ) (dip azimuth  $270 \angle 16^\circ$ ); this corresponds to the position of axis  $b$ . The angle between axis  $c$  and the translational-surface maximum was taken to be  $45^\circ$ .

With regard to the direction of the translation gliding, the orientation of the axes of the final strain ellipsoid was restored (Fig. 7). A similar situation was observed with the phlogopite orientations in these rocks (Fig. 7,  $b$ ); this is evidence for its growth during deformation. Microstructural studies suggest that the marbles were deformed by a simple strike-slip fault under N–S near-horizontal compression, during thrusting simultaneous with the formation of  $S_1$  and  $F_1$  macrostructures.

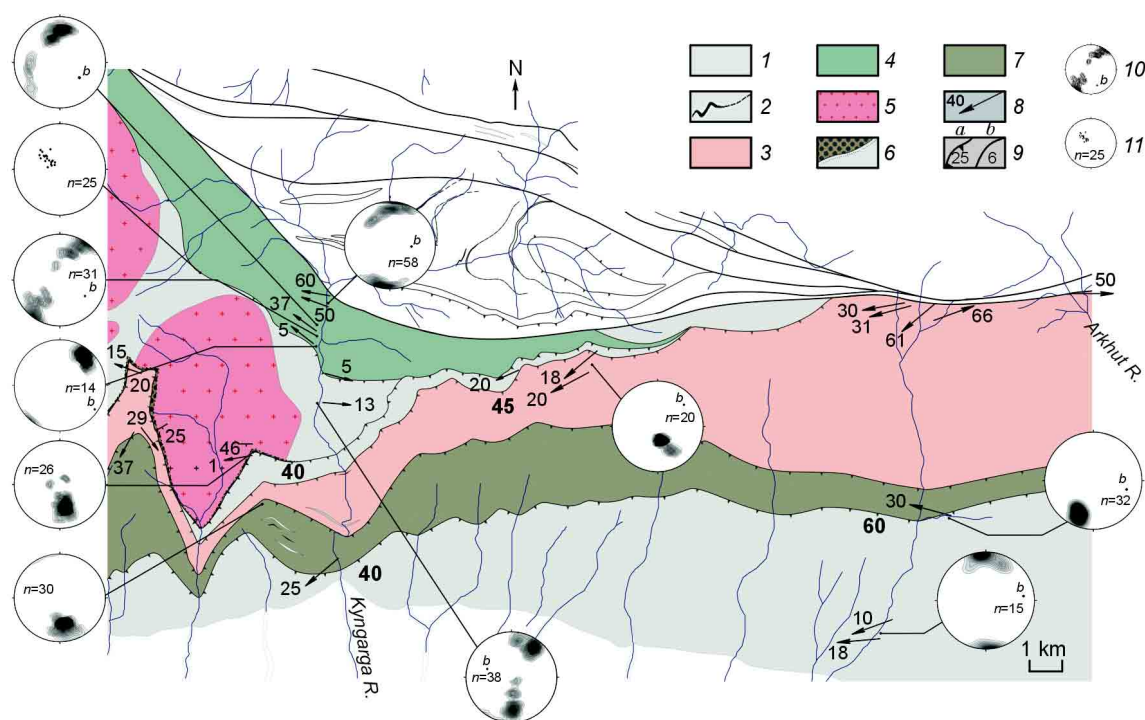


Fig. 4. Geological sketch map of the South Arshan domain. 1, marbles, calciphyres, quartz–carbonate mylonites, carbonaceous–carbonate mylonites; 2, marker bodies of garnet–mica schists; 3, amphibolites, garnet amphibolites, biotitic plagiogneisses, biotite–amphibole plagiogneisses; 4, metapelitic greenschists; 5, two-feldspar granites; 6, red-colored coarse-clastic rocks of the Sagan-Sair Formation; 7, diaphthoric greenschists; 8, fold-bend orientation; 9, faults: *a*, With an inclined fault plane; *b*, with a vertical fault plane; 10, bedding of the planar elements of schistosity and banding on the stereogram; 11, orientation of the long axes of deformed pebbles.

The amphibolite–gneiss tectonic sheet was studied in the Kyngarga River canyon and on the Bugatai–Bukhota and Bukhota–Kyngarga dividing crests. For sample T06031 of chloritized biotitic plagiogneiss (Pl, Qtz, Chl, Bt, Ep), taken from the left side of the Kyngarga River canyon, the orientation of chlorite, which conditioned the macroscopic planar structure of the rock (dip azimuth  $180 \angle 30^\circ$ ), was determined in an oriented thin section. The cleavage poles of chlorite on the stereogram formed an open rotational belt with the orientation of axis *b* (dip azimuth  $255 \angle 24^\circ$ ). This is due to the combination of two planar structures located at an acute ( $\sim 24^\circ$ ) angle with respect to each other (Fig. 8); the ratio between  $S_1$  and  $S_2$  (on the thin-section plane) suggests dextral movement. When we restore the sample orientation relative to the horizon and cardinal points, this indicates thrusting simultaneous with deformation. This microstructure resulted from a simple strike-slip fault under N–S near-horizontal compression, during thrusting simultaneous with the formation of  $S_2$  and  $F_2$  macrostructures.

On the Bugatai–Bukhota watershed, we observe the common schistosity of gneisses and garnet amphibolites with a sericitic  $S_2$  planar structure and small  $F_2$  folds. Here, sample F08217 of sericitized gneiss was taken (Fig. 9). The rock has a discontinuous cleavage, whose domains consist of fine-grained mica (sericite). The quartz and feldspar grains are crashed or turned, etc. The rock microstructure causes the appearance of macroscopic  $S_2$  schistosity.

### North Arshan domain

The North Arshan structural–lithologic domain consists of tectonic sheets made up of calcitic and calcite–muscovite marbles; quartz–carbonate and carbonaceous–carbonate mylonites; biotite–amphibole plagiogneisses (Fig. 10). The sheets are deformed and crumpled in an antiform with an E–W-striking bend surface. The rock metamorphism is intermediate between the greenschist and epidote–amphibolite facies (after metapelites). Chloritized biotitic plagiogneisses outcrop in the axial part of the structure. On the stereogram the orientation of gneissosity and banding forms a fold belt along the small-circle arc, with the bedding of the conic-fold bend (dip azimuth  $255 \angle 20^\circ$ ) (Fig. 10). The carbonate rocks in the antiform core are heavily deformed and represented by coarse-grained marbles and carbonate schists with small elongated calcite crystals. The limestones and dolomites of the Gorlyk Formation might have been the protoliths of these rocks. The marbles of the North Arshan domain have a complex folded structure. Two fold generations are distinguished. The  $F_1$  folds are relics of an isoclinal folded structure (Fig. 11, detached fold curves). The outcrops usually show a pseudomonoclinical structure, represented by  $S_1$  schistosity (parallel to the limbs of the  $F_1$  folds). This planar structure is deformed into a large  $F_2$  antiform owing to the bending of the axial surfaces and the limbs of the  $F_1$  folds, which are parallel to them. On the stereograms (Fig. 10), the schistosity

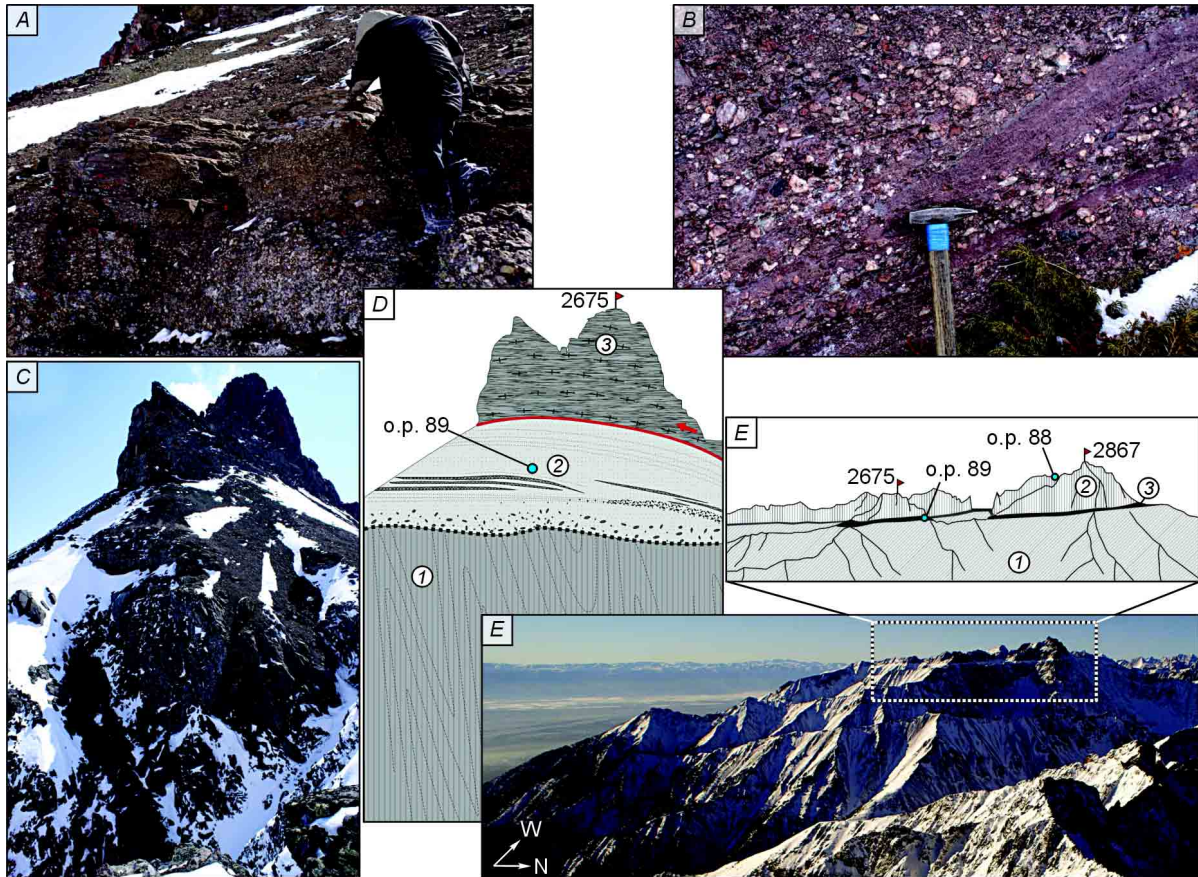


Fig. 5. Relationships between the Sagan-Sair Formation and the nappes. *a*, Gently ( $5^{\circ}$ – $10^{\circ}$ ) bedding conglomerates and sandstones in the upper reaches of the Tolta River; *b*, conglomerates and sandstones on the Bugatai–Bukhota watershed (dip angle  $25^{\circ}$ ); *c*, *d*, photo and sketch illustrating the overlap of deformed marble (1) by the Sagan-Sair Formation (2) and the location of the tectonic outlier, consisting of undulose gneisses (3); red line shows the location of the thrust plane; *e*, photo of the upper reaches of the Bugatai and Tolta Rivers, with a distinct thrust line in the topography; *f*, location of the autochthon (1), allochthon outliers (2), and outcrops of the coarse-clastic sediments of the Sagan-Sair Formation (3). o.p., Observation point.

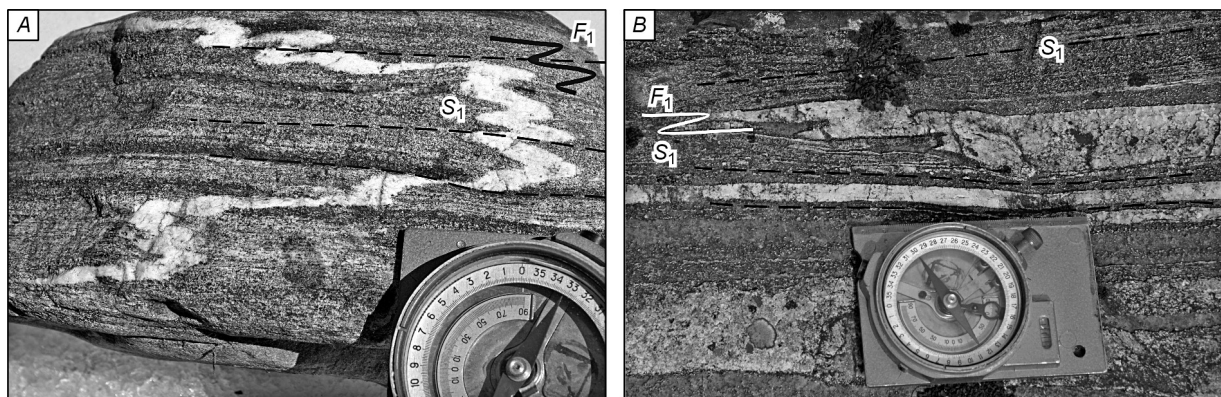


Fig. 6. Relationships between the  $F_1$  folds and the  $S_1$  planar structure of the first deformational stage. *a*, Ptygmatite folds (aplite vein) in biotitic plagiogneisses interbedded with amphibolites; *b*, shear-flow folds in marbles.

poles for the carbonates form a cylindrical fold in the western part of the area and a conic one in its eastern part. The bend surface of the antiform has a dip azimuth of  $192 \angle 60^{\circ}$ .

The antiform bend has dip azimuths of  $260 \angle 34^{\circ}$  in the west and  $274 \angle 18^{\circ}$  in the east. These values agree with the orientation of the bends of the small synchronous  $F_2$  folds.

The schistosity geometry in the marbles of the North Arshan domain (Fig. 10) can be interpreted as the periclinal closure of a cylindrical antiform or as a result of superimposed inhomogeneous deformation. The observed geologic structure and orientation of the bend suggest that the structure closed in the west, not in the east, contrary to the observations. Thus,

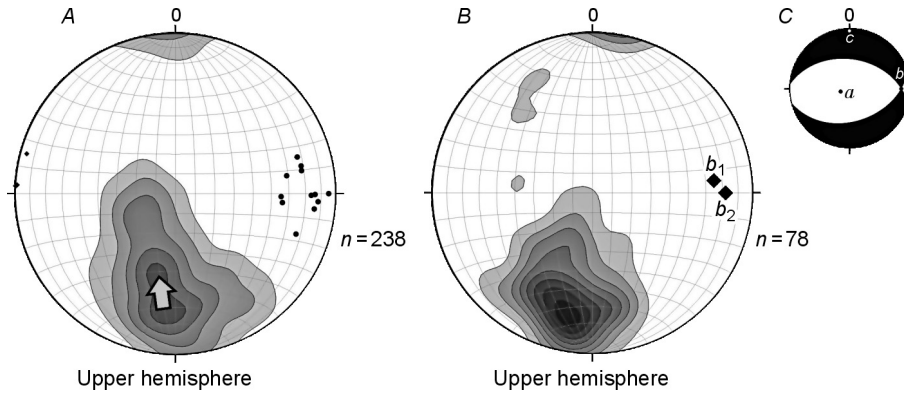


Fig. 7. Stereograms of the orientations of the translational twins of calcite  $e(01\bar{1}2)$  (a) and phlogopite crystals (cleavage) (b), with a dynamic microstructural interpretation (c). a, Arrow shows the direction of twin sliding, and dots show the fracture bends of the calcite twins; b,  $b_1$ , rotational axis, obtained from the micas;  $b_2$ , rotational axis, obtained from the calcite twins; c, hereinafter, compression areas are shown in black and extension ones are shown in white.

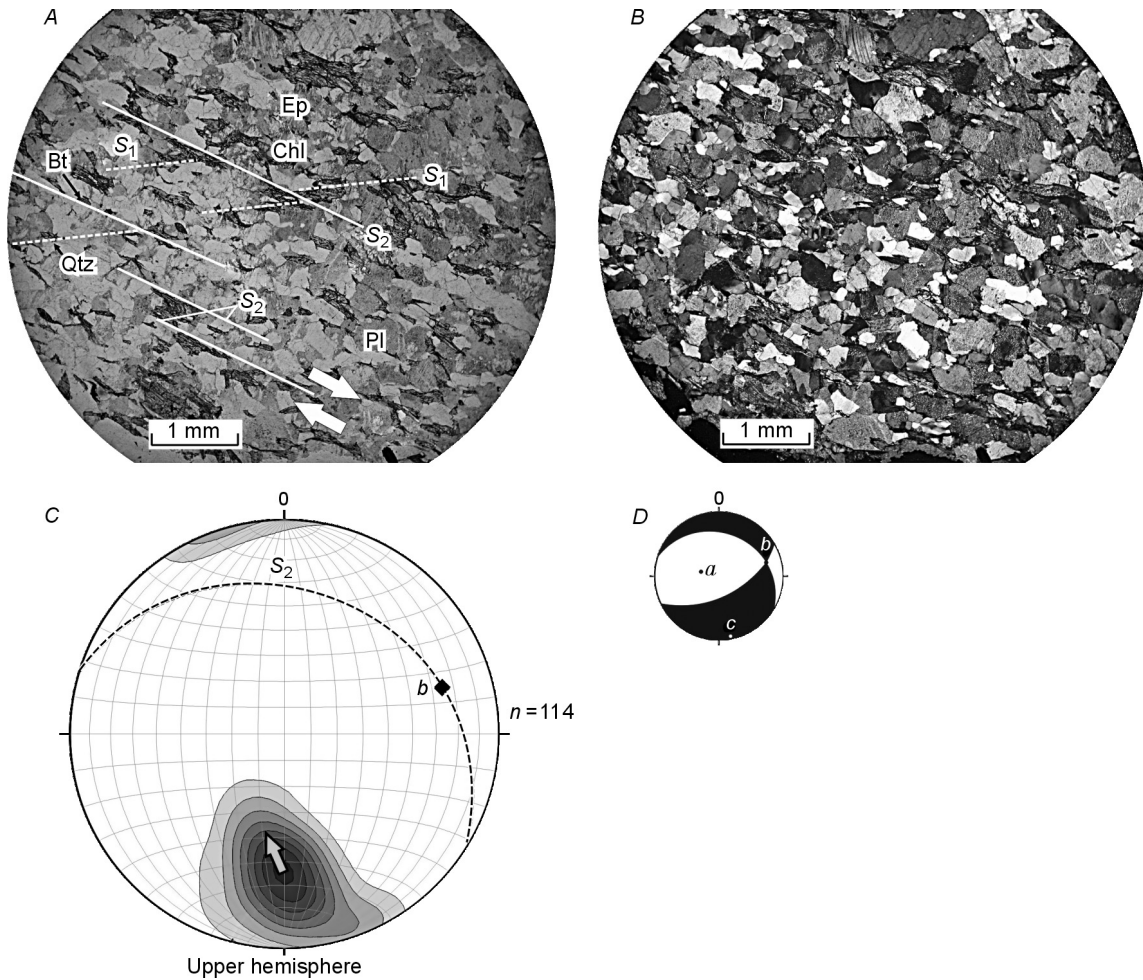


Fig. 8. Chlorite orientation in chloritized plagiogneiss. a, b, Rock micrographs: a, Nicols II; b, nicols  $\times$ ; c, stereogram of the chlorite orientations, dashed line shows the  $S_2$  sliding plane; arrow shows the sliding direction; d, dynamic microstructural interpretation.

the antiform is conic in the east most probably because of the inhomogeneous deformation of a cylindrical structure. The marbles contain sheets of carbonaceous schists (Bt, Qtz,  $\pm$ Grt,  $\pm$ Mus,  $\pm$ Graph), which delineate the folded structure of the North Arshan domain (Fig. 10).

**Microstructural analysis of the metamorphic rocks from the North Arshan domain**

The marbles of the North Arshan domain contain tectonic sheets of biotitic gneisses, which are part of the folded

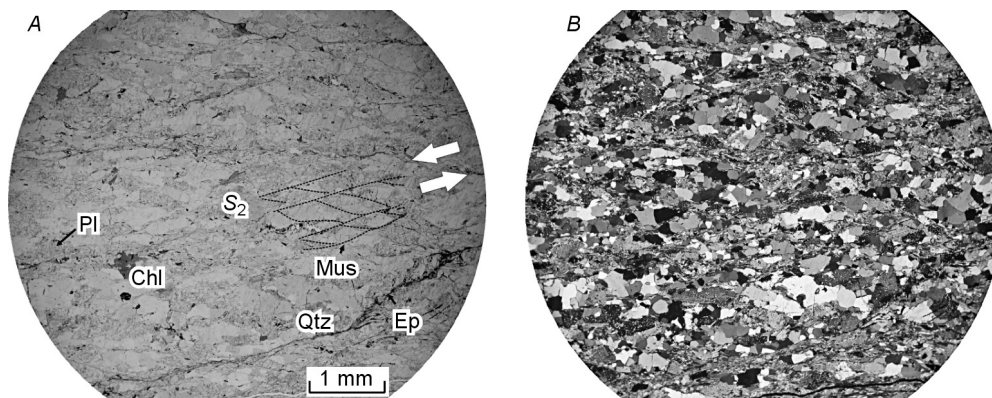


Fig. 9. Micrographs of sericitized plagiogneiss. *a*, Nicols II; *b*, nicols  $\times$ . The structure of quartz and feldspar grains enveloped by an aggregate of fine-grained muscovite (reticular schistosity) yields the  $S_2$  macroscopic sliding plane; arrows show the direction of sliding on the thin-section plane.

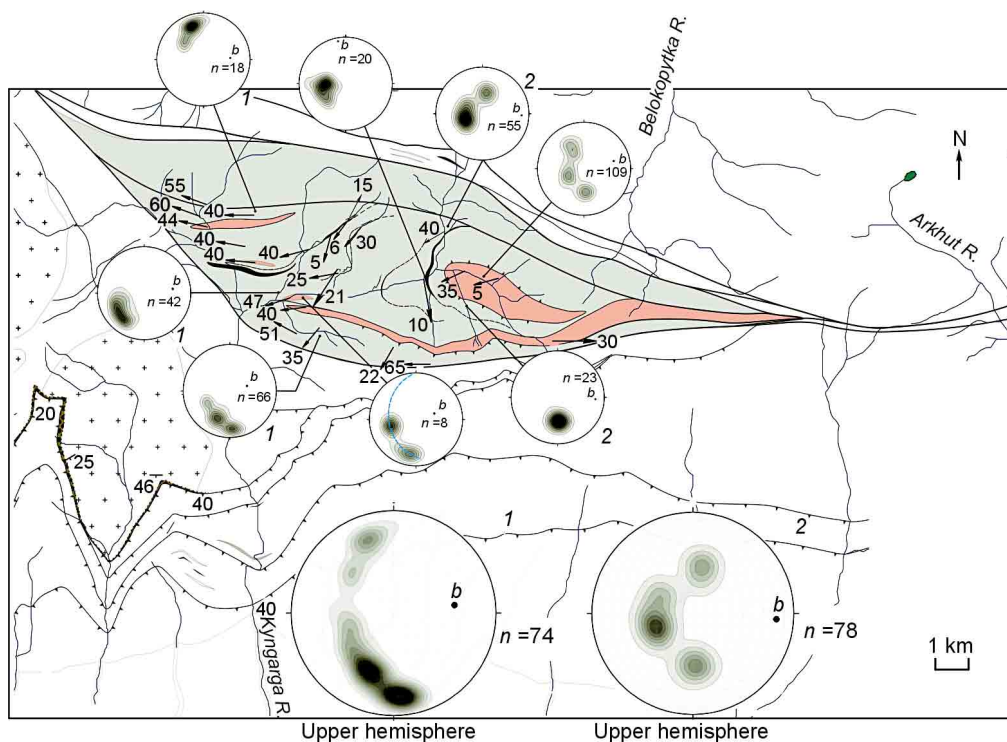


Fig. 10. Geological sketch map of the North Arshan domain. See legend in Fig. 4. Composite stereograms show schistosity in the marbles and carbonate mylonites in the western (1) and eastern (2) parts of the structure.

structure. These sheets were studied in the Kyngarga River valley and in the canyons of its tributaries.

The mica orientation was determined in a thin section for sample T08007 of biotitic plagiogneiss (Pl, Qtz, Bt, Ep), taken from the right side of the Kyngarga River canyon, east of the arrows of the right and left tributaries (Fig. 12, *a*). The outcrops of the cleavage normals form an open rotational belt (*b*-tectonite), suggesting the presence of several (in this case two) shear systems, located at an acute angle with respect to each other. The rotational axis is close to the bend of the  $F_2$  antiform. This suggests that the rock was deformed by a strike-slip fault (with elements of rotation around an axis with a dip azimuth of  $250 \angle 41^\circ$ ), simultaneously with the formation

of the  $F_2$  folded structures. The gneiss outcrops are confined to the antiform core.

A similar mica orientation was obtained for sample T09001 of biotitic plagiogneiss (Pl, Qtz, Bt, Ep). The tectonic sheet which the oriented sample was taken from is located on the northern limb of the  $F_2$  antiform. The rocks have a distinct aggregate *b*-linearity, which is manifested in the orientation of the quartz–feldspar rods ( $\varnothing 1\text{--}2$  mm, elongation 1/5), surrounded by mica scales. On the stereogram the outcrops of the cleavage normals form a homogeneous rotational belt (Fig. 12, *b*).

This suggests that rotation here played a greater role in the deformation than in sample T08007. This difference in the

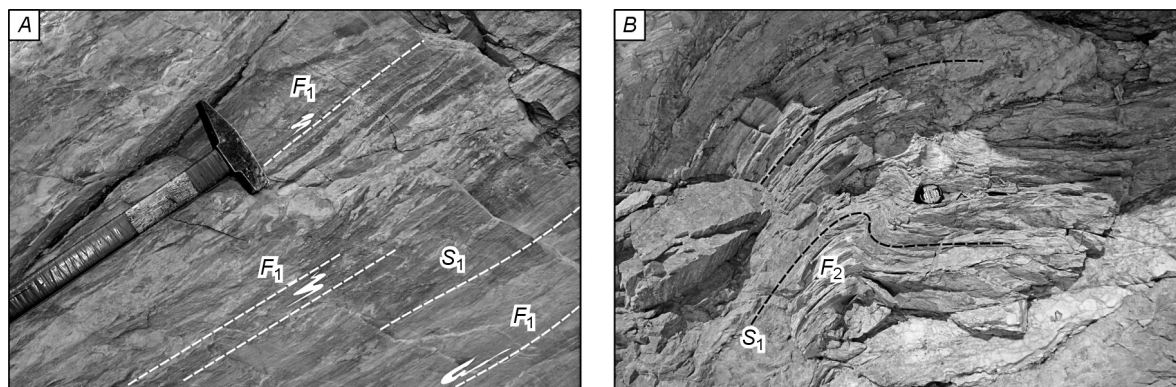


Fig. 11. Morphology of the  $F_1$  and  $F_2$  folds in the marbles from the North Arshan domain. *a*,  $F_1$ ; *b*,  $F_2$ . The  $F_1$  folded structures are highly disharmonious.

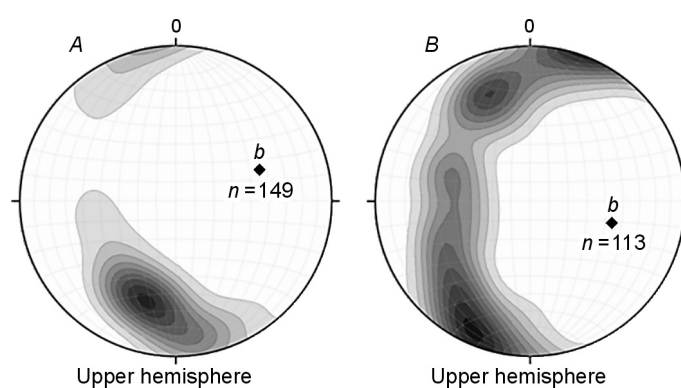


Fig. 12. Stereograms of the orientations of the biotite crystals in the gneisses. *a*, Sample T08007; *b*, sample T09001.

microstructural anisotropy of the rocks identical in the mineral composition is due to the different position of these geologic bodies in the large folded structure. Apparently, the formation of the belt *b*-tectonites results from a simple strike-slip fault during interlaminar sliding simultaneous with the bending of the tectonic-sheet complex and the formation of the large  $F_2$  antiform. Note that the rocks located on the flanks of the structure experienced stronger deformations than those in the core owing to the larger sliding amplitude. This explains the fundamental microstructural differences between the *b*-tectonites in different parts of the North Arshan domain.

The following was observed in studies of schist sheets in the marbles (Bt, Qtz,  $\pm$ Grt,  $\pm$ Mus,  $\pm$ Graph). The garnet crystals in these rocks have “snowball” structures owing to captured carbonaceous matter and biotite scales as well as asymmetric “pressure shadows,” consisting of a fine-grained quartz aggregate (Fig. 13). This suggests that the minerals grew during deformation with elements of rotation (strike-slip fault). These microstructural observations, along with the macrostructural orientation in the schists, might be evidence for syntectonic growth of garnet and biotite under a simple strike-slip fault during interlaminar sliding simultaneous with the formation of the  $F_2$  antiform.

Sample T09053 of quartz–carbonate–muscovite schist (Qtz, Cal, Mus,  $\pm$ Ep,  $\pm$ Scap) was taken from the left side of the

Kyngarga River canyon, near the confluence of the right and left tributaries, to study the mica (muscovite) orientation (oriented sample) (Fig. 14). The rocks are located on the southern limb of the large  $F_2$  antiform.

The outcrops of the cleavage normals form an open rotational belt (*b*-tectonite), suggesting the presence of several (in this case two) shear systems, located at an acute angle with respect to each other. The rotational axis is close to the bend of the  $F_2$  antiform. Microstructures such as mica fish and the microdisplacement direction during the deformation of calcite crystals suggest reverse faulting, which corresponded to counterclockwise rotation around axis *b* up the dip of the bend.

These microstructural data might suggest that differential sliding took place during the formation of the  $F_2$  antiform, on its limbs. It is inevitable during the formation of a large folded structure with an angle of  $\sim 50^\circ$  between the flanks, because it is impossible to solve the problems of space shortage in the core and its “excess” in the curve (outer core) only by the formation of micro- and mesostructures (cleavage and strolites in the first case and tension cracks in the second one). During the deformation the folded structure, under external forces, tries to pass from the orthogonal type to this one by matter redistribution between the fold core and limbs.

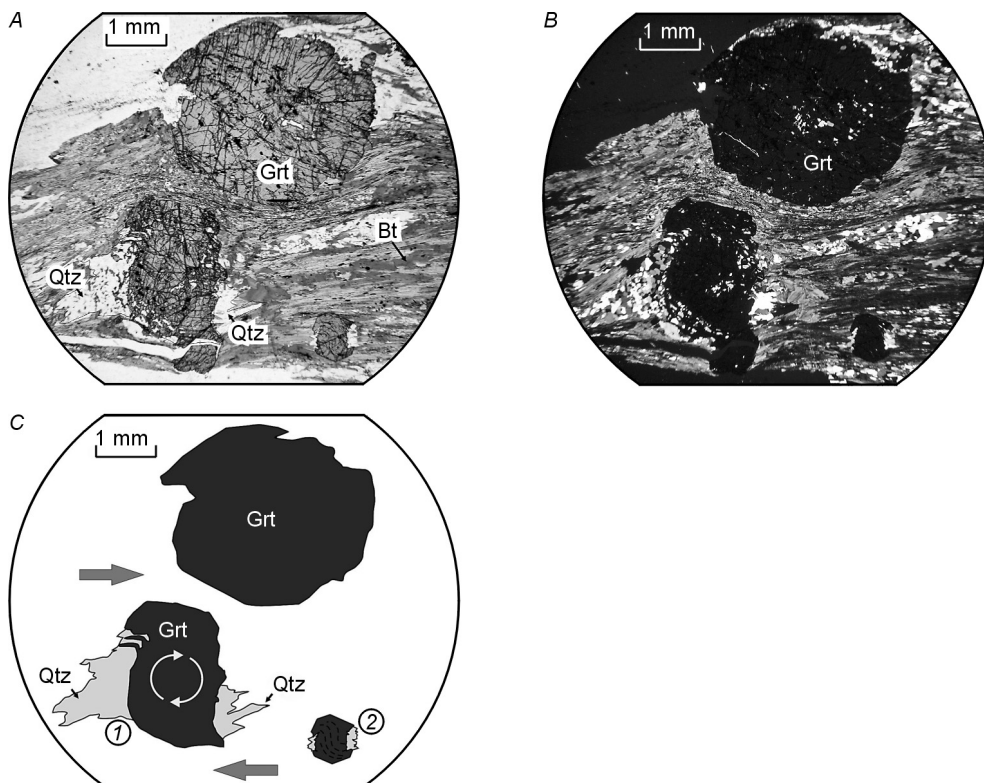


Fig. 13. Micrographs of quartz–garnet–biotite schist (sample T08016). *a*, Nicols ll; *b*, nicols x; *c*, kinematic microstructural interpretation: 1, asymmetric quartz “pressure shadows” around a garnet porphyroblast; 2, inclusions in a porphyroblast forming a “snowball” structure.

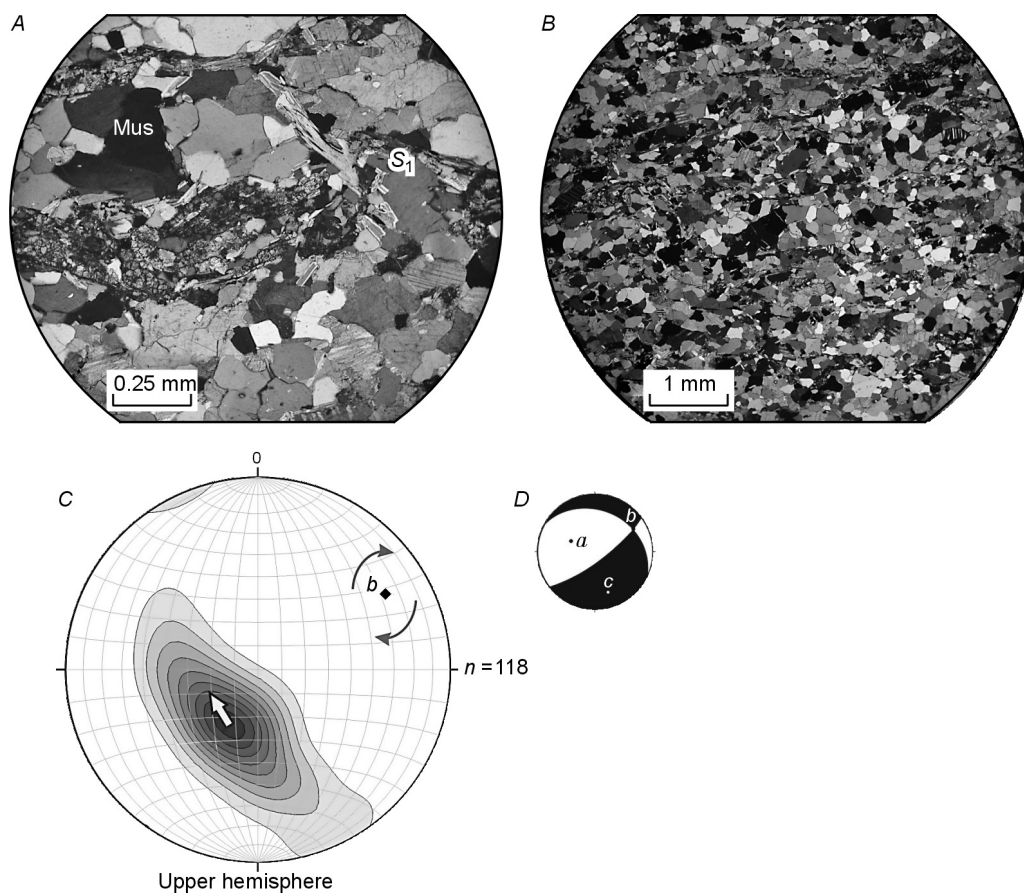


Fig. 14. Muscovite orientation in quartz–carbonate–muscovite schist (sample T09053). *a*, *b*, Micrographs: *a*, Nicols ll; *b*, nicols x; *c*, stereogram of muscovite orientations; heavy arrow shows the direction of differential sliding; *d*, dynamic microstructural interpretation.

### Strike-slip fault zones at the Arshan reference locality

The geologic boundaries of the North Arshan domain are strike-slip fault zones. The northern tectonic contact (Fig. 15, number 2) is reflected in the formation of a bend “fan” (with an increasing dip angle toward the fault) in the greenschists, the formation of  $S_3$  schistosity and fault-line  $F_3$  folds, followed by the growth of poikilitic amphibole crystals on plane  $S_3$ . The macro- and microstructural data point to sinistral strike-slip shearing. In the north of the area, in the watershed part of the ridge, the North Arshan domain is truncated by the strike-slip fault zone of the Arkhut–Kynygarga fault (Fig. 15, number 3). The fault zone was traced from east to west from the Arkhut River valley to the watershed of the Kynygarga and Fedyushka Rivers. It contains tectonic blocks/sheets consisting of carbonate mylonites, undulose microcline granites, plagiogneisses, amphibolites, and serpentinites.

The marbles in the fault zone are heavily deformed. The  $S_3$  schistosity in them is conformable to the general strike of the tectonic zone with a dip azimuth averaging  $16 \angle 86^\circ$ . The rock corrugation and the bends of the small folds dip steeply. The carbonate mylonites contain lenticular marble boudins. On the basis of morphology, this structural type is identified as ductile-flow boudinage. This might suggest that the forma-

tion of these structures was almost simultaneous with the folding and metamorphism.

The amphibolites in the fault zone are represented by plagioclase–amphibole and garnet–plagioclase–amphibole varieties (Fig. 16, a). The schistosity, determined by the orientation of flattened amphibole crystals, forms a compact halo on the stereographic projection, with a dip azimuth averaging  $19 \angle 87^\circ$ . At the microscopic level, the rocks were studied by measuring the crystallographic lines of the amphibole crystals and restoring the predominant crystal orientation from them. The cleavage of greenish blue hornblende {110} and the jointing across elongation {001} were measured in oriented thin sections. On the stereogram the points of the cleavage poles are scattered in a sector, with an angle of  $\sim 90^\circ$ , forming two distinct maxima (Fig. 16, b), which correspond to two cleavage directions in a normal amphibole crystal. The jointing poles form one distinct maximum. Since the cleavage poles form a sector, not a rotational pole, amphibole shows most probably  $a$ -linearity. Axis  $c$  is perpendicular to schistosity, and the orientation of axis  $b$  is restored from the orientation of axes  $a$  and  $c$ .

The gneisses and plagiogranites in the Arkhut–Kynygarga fault are heavily undulose and mylonitized, with a planar directional structure ( $S_3$ ). On the stereogram, the  $S_3$  normals

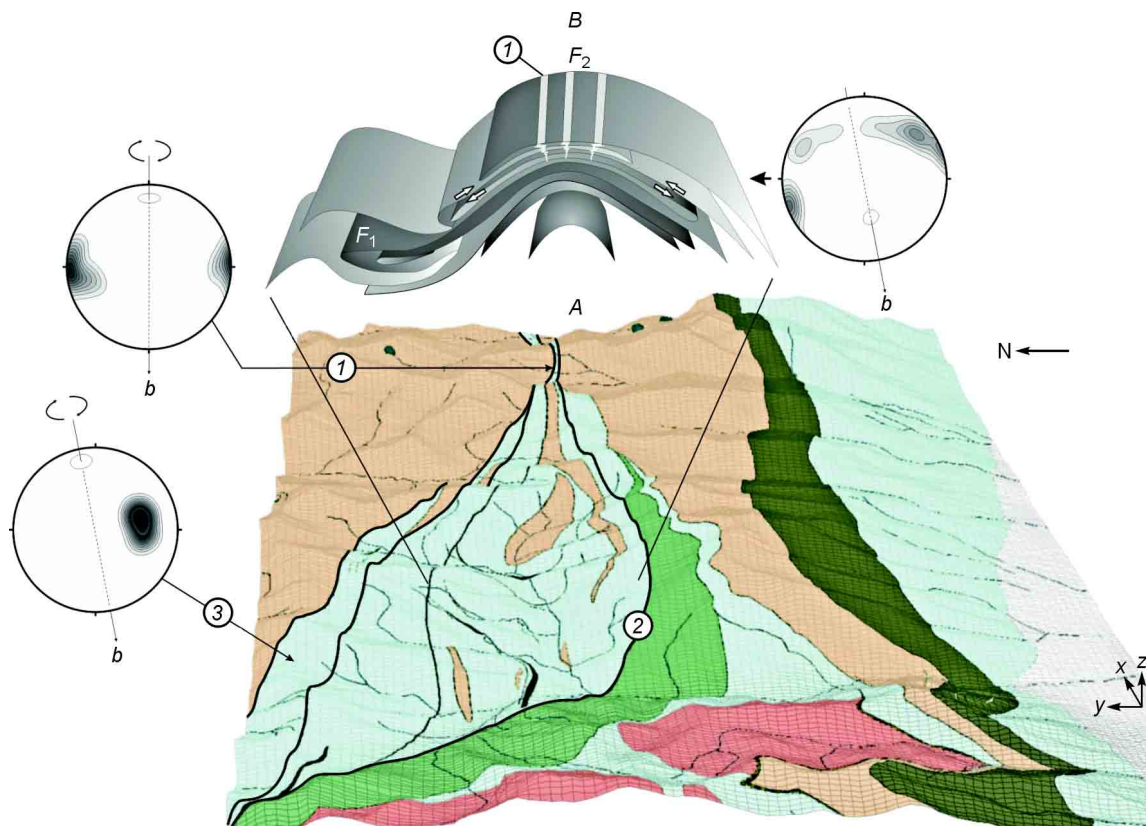


Fig. 15. 3D geological map of the reference locality (A), with a structural block diagram for the North Arshan domain (B). A: 1, hydrothermal-vein accumulations, confined to an antiform curve; 2, shear zone between the North and South Arshan domains; 3, Arkhut–Kynygarga fault. Isolines show the density of the schistosity normals (projection plane is normalized to “pseudo 3D” plane  $xz$ ); line shows the orientation of rotational axis  $b$ . B: 1, location of the shear zones in the nappe structure of the area.

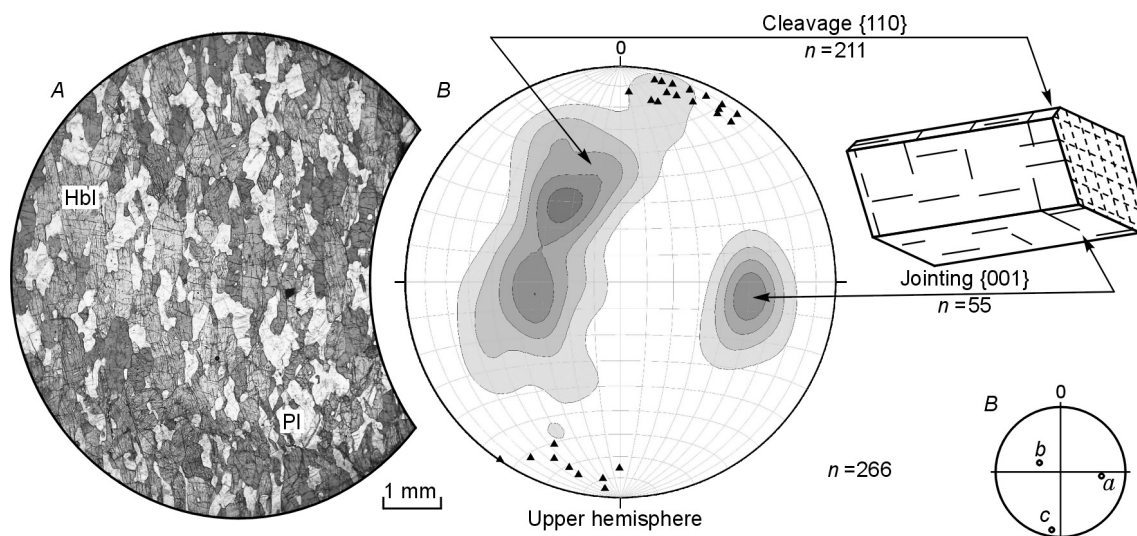


Fig. 16. Micrographs of amphibolite sample T09044 (a); stereogram of the orientations of the cleavage and jointing of the amphibole crystals (b); location of the axes of the final strain ellipsoid on the stereogram (c). Triangles show poles of macroscopic schistosity.

form a compact halo with the maximum dip azimuth of  $354 \angle 86^\circ$ .

#### Geodynamic model for the deformation in the Arshan area

Dynamic analysis, combined with the Ar–Ar dating of the syntectonic minerals (micas, amphiboles), permitted constructing a geodynamic model for the formation of the Late Paleozoic nappe structures at the Arshan reference locality.

**Thrust faults (316–310 Ma).** The structures of the thrust-fault stage are best preserved in the South Arshan domain. Macrostructurally, they are “monoclinical” tectonic sheets with S-dipping tectonic contacts. They show intense shear-flow folding ( $F_1$ ). Also,  $a$ -linearity and  $S_1$  planar structure are widespread. The former is represented by the orientation of elongated amphibole crystals. The latter is determined in the amphibolites by the orientation of melano- and leucocratic bands and flattened amphibole crystals; in the marbles, by that of smoothed calcite crystals. In general, these structures formed during near-N–S compression (Fig. 17). Different sheets show very close results of the dynamic analysis, suggesting cohesive macroscopic deformations. Thus, this stage is marked by deformations typical of thrusting environments. Judging by the fold kinematics, the deformations began most probably in the amphibolite facies. However, most of the parageneses correspond to the epidote–amphibolite facies, and this points to the environment in which the structures of this stage finished their formation. In our case dating is possible for the syntectonic minerals, which form corresponding linear planar structures (amphibole, biotite). Amphibole from the garnet (sample 06-90-3) and plagioclase–biotite (samples 07-51, 06-90-1) amphibolites is  $315.2 \pm 3.5$ ,  $316.5 \pm 3.3$ , and  $316.1 \pm 3.2$  Ma, respectively (Fig. 18, plateau

age). Biotite from sample 06-94, which forms  $S_1$  planar structure in the greenschist sheet, is  $310.7 \pm 3$  Ma old.

**Fold deformation (305–303 Ma).** The structures of the fold deformation stage are widespread at the reference locality and the most abundant in the North Arshan domain. Here, compositionally different tectonic sheets form a cylindrical antiform with an angle of  $\sim 50^\circ$  between the limbs and a gently W-dipping ( $20$ – $30^\circ$ ) bend. The previous-stage ( $F_1$ ) folded structures occur only as relics among numerous small  $F_2$  folds resulting from interlaminar sliding simultaneous with the general bending. Dynamic analysis (Fig. 19) suggests that the external forces almost did not change their orientation as compared with the previous stage (Fig. 17). The only difference is the change in the dip of the rotational axis and its general westward inclination.

Syntectonic biotite from sample 06-95 of quartz–garnet–biotite schist in the antiform core yielded a plateau age of  $303.1 \pm 3.0$  Ma, coeval with the antiform in the North Arshan domain. The deformation took place during epidote–amphibolite metamorphism. In the South Arshan domain, the second-stage structures are manifested in small or medium-sized ductile-fracture and shear folds ( $F_2$ ) as well as  $S_2$  planar structure, consisting of micas and chlorites. Fine-grained muscovite from sample F08217, located microstructurally in  $S_2$  cleavage domains (Fig. 9), yielded a plateau age of  $304.8 \pm 3.3$  Ma. Biotite ( $S_2$ ) from sample 07-51 of plagioclase–biotite schistose amphibolite is  $303.0 \pm 2.8$  Ma old (Fig. 18).

According to structural and geological data, dynamic analysis, and Ar–Ar dating, stability is lost and the deformation concentrates in a relatively narrow linear zone (now the North Arshan domain) in this stage, at a macroscopic level. This corresponds to a transition from nappe to fold–thrust structures, in which the tectonic sheets themselves are involved in the folding.

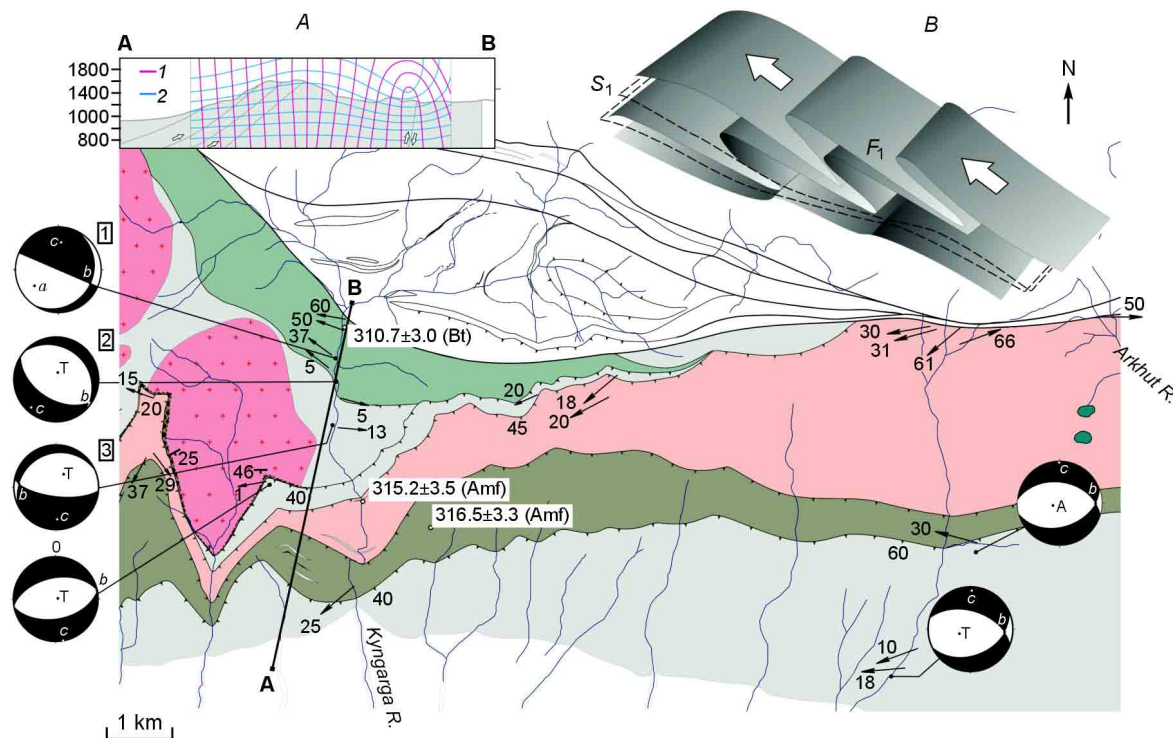


Fig. 17. Geological sketch map of the South Arshan domain, with the results of the dynamic analysis of the macro- and microstructures for the first deformation stage in the area. *a*, Section along line A–B shows reconstructed trajectories describing plateaux of normal strains  $\sigma_3$  (1) and  $\sigma_1$  (2); *b*, block diagram for the predominant structural forms. The sketch shows the Ar–Ar ages of the minerals forming the microstructures in this stage. See legend in Fig. 4.

**Strike-slip faults (286 Ma).** The structures of the strike-slip fault stage are localized in narrow linear zones cutting older structures. They characterize the subsequent deformation of the studied geologic bodies along strike-slip faults of different kinematics. Within the fault zones, the deformations were manifested in  $S_3$  planar structure and  $F_3$  folds. Also, this stage was marked by the inhomogeneous deformation of the older folded structures ( $F_1$ ,  $F_2$ ), including those outside the fault zones. This was manifested in the deformation of the North Arshan antiform, which acquired a conic geometry in its eastern part. Note that this large folded structure is bounded by strike-slip faults: by the Arkhut–Kyngarga dextral strike-slip fault in the north and by a sinistral strike-slip fault in the south. These facts in combination might suggest the inhomogeneous deformation of the  $F_2$  antiform and the westward “squeezing” of the North Arshan domain along adjacent dextral and sinistral strike-slip faults (Fig. 20). The observed variations in the orientations of the compression and extension axes for this stage (Fig. 20) are mainly due to the considerable inhomogeneity of the existing geologic structures and characterize the described mechanism of squeezing tectonic blocks along systems of adjacent faults. This gives rise to  $S_2$  schistosity and  $F_3$  folds with steeply dipping ( $60$ – $70^\circ$ ) bends. Amphibole (sample 6-94) on plane  $S_3$  is  $286.8 \pm 4.8$  Ma old.

Note that all the described types of structures might have formed by the same compressive forces at  $316$ – $286$  Ma. This is evidenced by the facts that the arrangement of the reconstructed compression and extension areas for structures of types I and II (Figs. 17, 19) is almost similar and all the

ages (with regard to the confidence interval) overlap completely.

Studies of the structural forms at the Arshan reference locality suggest the widespread occurrence of Late Paleozoic ( $C_3$ – $P_1$ ) structures in the southeastern segment of the Sayan–Baikal Fold Region. First and foremost, the deformations took place near the source of the forces which caused them or in the structures which concentrated strains. The latter are exemplified by the MSF, which separates the marginal basement inliers of the southern Siberian Platform from its folded framing. The reference locality lies approximately 20 km south of the MSF. The syntectonic granitoids in the MSF are  $353$ – $278$  Ma old (U–Pb, Rb–Sr) (Savel’eva et al., 2006, 2010), and the syntectonic metasomatic rocks are  $321$ – $309$  Ma old (Ar–Ar) (Savel’eva et al., 2003). These dates overlap completely with the age of the nappes at the Arshan reference locality. Thus, the shear and thrust structures formed simultaneously.

Interestingly, the deformations at a relatively short distance took place in many ways: along the marginal suture by the strike-slip fault mechanism with movements on the horizontal plane of the MSF; farther south, mainly by thrusting. These facts dismiss the question which structures are primary in the region, the thrust or shear ones. This question is meaningless if unrelated to specific structural units (blocks, structural domains, etc.) forming a force scheme. In some cases we see older strike-slip faults and younger thrusts; in other cases, vice versa. Note the inhomogeneity of the geologic environment, caused by the previous stages of tectogenesis (in this case

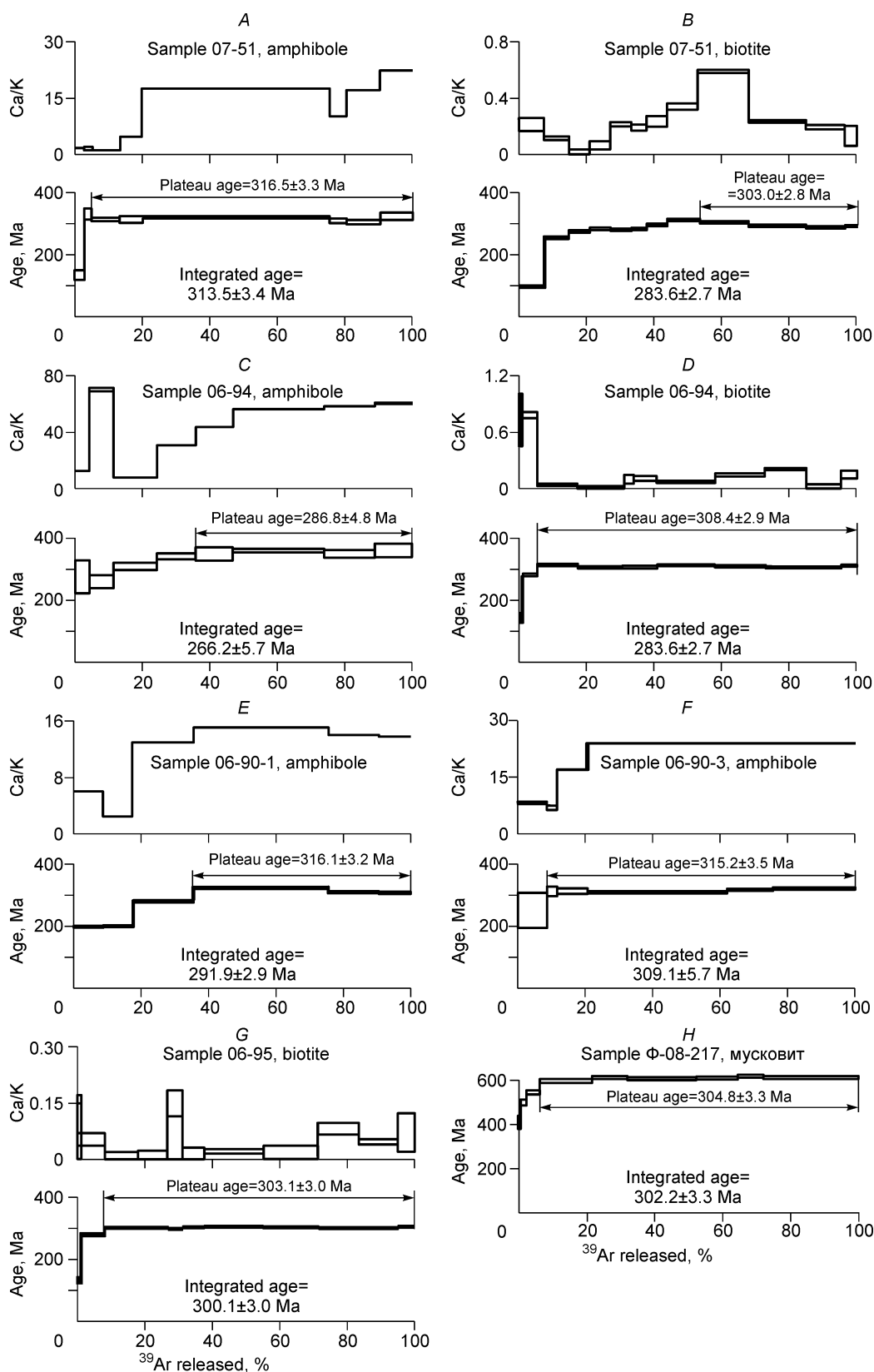


Fig. 18. Ar–Ar ages of the syntectonic minerals from the rocks of the Arshan area. A, D–F, Ar–Ar spectra of the minerals forming the microstructures in the first (thrust-fault) stage; B, G, H, Ar–Ar spectra of the minerals forming the microstructures in the second (fold deformation) stage; C, amphibole along the planes of *S*<sub>3</sub> schistosity, formed in the third (strike-slip fault) stage.



Caledonian), and, correspondingly, the diversity of local dynamic settings (force schemes). The same compressive forces operating at some moment at different points give rise to different structures.

## Conclusions

The Late Paleozoic nappe complexes in the Tunka bald mountains are an example of complex structures resulting from intracontinental deformations.

The Alps and the Himalayas are typical nappe regions, with so-called “thin-skinned” tectonics. Here, the nappes develop on an essentially homogeneous substrate with a relatively simple structure, consisting of the Mesozoic and Cenozoic sedimentary strata. Now the methods for studying the geology of such structures are well-developed and widely used in applied and basic research (Bose et al., 2009).

However, many folded structures form on a substrate which has experienced at least one thrusting and folding stage (areas with “thick-skinned” tectonics). Here, the deformations take place on an extremely inhomogeneous substrate with complex anisotropy. The Tunka bald mountains are an example of nappe structures which include older deformational complexes. Since they have a complex structure and diverse structural forms, there is no universal method for studying them yet. By methods of structural geology, microtectonics, and radioisotopic dating, this study has solved some problems concerning the structure and the kinematic and dynamic conditions needed for the formation of the Late Paleozoic structures in the Tunka bald mountains. It has been found that the thrust and shear structures (the thrusting in the south and the displacement along the MSF in the north of the region) developed almost simultaneously. The relationships between these structures in the Arshan area can serve as the basis for a working model in studying the widespread thrust and shear structures in the southwestern folded framing of the Siberian craton. The thrusting in the Tunka bald mountains was coeval with the major shear structures in the eastern Central Asian Fold Belt (MSF; Kurai, Northeastern, and Irtysh crumpled zones, etc.) (Buslov et al., 2003). Also, it was simultaneous with the formation of continental-margin calc-alkalic and shoshonite series (305–278 Ma) as well as that of the alkali and alkali-feldspar syenites and granites (281–278 Ma) of the Tarim mantle plume in the Angara–Vitim pluton, located near and east of the studied region (Borisenko et al., 2006; Dobretsov et al., 2010; Tsygankov et al., 2010). Thus, the simultaneous development of the Late Paleozoic structures, active-margin structures, and plume magmatism in southern Siberia might have resulted from the global geodynamic events caused by the interaction between the tectonic plates which formed the Central Asian Fold Belt.

The paper is based on the dissertation prepared for defense by A.B. Ryabinin, who tragically perished on 7 January 2010 on the Ivannikov Passage (Tunka bald mountains). He had celebrated his 26th birthday the day before. Aleksandr Ryabinin was a kind and friendly person. He passionately loved

the mountains, their beauty and geological mysteries, some of which he managed to solve.

## References

- Anisimova, S.A., Geletii, N.K., Barash, I.G., 2010. Biofacies description of the sedimentary cover on the eastern margin of the Tuva–Mongolian microcontinent, in: *Geodynamic Evolution of the Lithosphere of the Central Asian Mobile Belt (from Ocean to Continent) (14–17 October 2010, Irkutsk)* [in Russian]. IZK SO RAN, Irkutsk, Vol. 1, pp. 19–20.
- Belichenko, V.G., Boos, R.G., Kolosnitsina, T.N., Lepin, V.S., Solodyankina, V.N., Snytko, A.V., 1988. New data on the age of the metamorphic series in the Tunka bald mountains (East Sayan). *Dokl. Akad. Nauk SSSR* 301 (2), 402–405.
- Belichenko, V.G., Sklyarov, E.V., Dobretsov, N.L., Tomurtogoo, O., 1994. Geodynamic map of Paleasian Ocean: Eastern segment. *Geologiya i Geofizika (Russian Geology and Geophysics)* 35 (7–8), 29–40 (22–32).
- Belichenko, V.G., Reznitsky, L.Z., Geletii, N.K., Barash, I.G., 2003. Tuva–Mongolia terrane (in the context of microcontinents in the Paleasian ocean). *Geologiya i Geofizika (Russian Geology and Geophysics)* 44 (6), 554–565 (531–541).
- Boos, R.G., 1991. The Paleozoic in the Tunka Bald Mountains, East Sayan [in Russian]. Nauka, Novosibirsk.
- Borisenko, A.S., Sotnikov, V.I., Izokh, A.E., Polyakov, G.V., Obolensky, A.A., 2006. Permo-Triassic mineralization in Asia and its relation to plume magmatism. *Russian Geology and Geophysics (Geologiya i Geofizika)* 47 (1), 170–186 (166–182).
- Bose, S., Mandal, N., Mukhopadhyay, D.K., Mishra, P., 2009. An unstable kinematic state of the Himalayan tectonic wedge: Evidence from experimental thrust-spacing patterns. *J. Struct. Geol.* 31 (1), 83–91.
- Buslov, M.M., 2011. Tectonics and geodynamics of the Central Asian Foldbelt: the role of Late Paleozoic large-amplitude strike-slip faults. *Russian Geology and Geophysics (Geologiya i Geofizika)* 52 (1), 52–71 (66–90).
- Buslov, M.M., Watanabe, T., Smirnova, L.V., Fujiwara, I., Iwata, K., De Grave, J., Semakov, N.N., Travin, A.V., Kir'yanova, A.P., Kokh, D.A., 2003. Role of strike-slip faulting in Late Paleozoic–Early Mesozoic tectonics and geodynamics of the Altai–Sayan and East Kazakhstan regions. *Geologiya i Geofizika (Russian Geology and Geophysics)* 44 (1–2), 49–75 (47–71).
- Buslov, M.M., Ryabinin, A.B., Zhimulev, F.I., Travin, A.V., 2009. Manifestations of the Late Carboniferous and Early Permian stages of formation of nappe–fold structures in the southern framework of the Siberian platform (East Sayany, South Siberia). *Dokl. Earth Sci.* 428 (7), 1105–1108.
- Butov, Yu.P., Minina, O.R., Neberikutina, L.M., Tregub, T.F., Katyukha, Yu.P., 2001. The Sagan-Sair Formation as a standard Late Paleozoic–Mesozoic molasse in the Buryatian East Sayan. *Vestn. Voronezhsk. Univ., Geologiya*, No. 12, 87–101.
- Dobretsov, N.L., 1985. A model for the East Sayan nappe tectonics. *Geotektonika*, No. 1, 39–50.
- Dobretsov, N.L. (Ed.), 1988. *Geology and Metamorphism of the East Sayan* [in Russian]. Nauka, Novosibirsk.
- Dobretsov, N.L., Buslov, M.M., 2007. Late Cambrian–Ordovician tectonics and geodynamics of Central Asia. *Russian Geology and Geophysics (Geologiya i Geofizika)* 48 (1), 71–82 (93–108).
- Dobretsov, N.L., Borisenko, A.S., Izokh, A.E., Zhmodik, S.M., 2010. A thermochemical model of Eurasian Permo-Triassic mantle plumes as a basis for prediction and exploration for Cu–Ni–PGE and rare-metal ore deposits. *Russian Geology and Geophysics (Geologiya i Geofizika)* 51 (9), 903–924 (1159–1187).
- Donskaya, T.V., Sklyarov, E.V., Gladkochub, D.P., Mazukabzov, A.M., Sal'nikova, E.B., Kovach, V.P., Yakovleva, S.Z., Berezhnaya, N.G., 2000. The Baikal collisional metamorphic belt. *Dokl. Earth Sci.* 374 (7), 1075–1079.

- Fedotova, A.A., Khain, E.V., 2002. Tectonics of the southern part of Eastern Sayan and its tectonic position in the Urals–Mongolian Belt, in: Leonov, Yu.G. (Ed.), *Trans. Geol. Inst.* [in Russian]. Nauchnyi Mir, Moscow, Issue 537.
- Gladkochub, D.P., Donskaya, T.V., Fedorovsky, V.S., Mazukabzov, A.M., Larionov, A.N., Sergeev, S.A., 2010. The Olkhon metamorphic terrane in the Baikal region: An Early Paleozoic collage of Neoproterozoic active margin fragments. *Russian Geology and Geophysics (Geologiya i Geofizika)* 51 (5), 447–460 (571–588).
- Kotov, A.B., Sal'nikova, E.B., Reznitskii, L.Z., Vasil'ev, E.P., Kozakov, I.K., Yakovleva, S.Z., Kovach, V.P., Berezhnaya, N.G., 1997. Age of metamorphism of the Slyudyanka crystalline complex, southern Baikal area: U–Pb geochronology of granitoids. *Petrology* 5 (4), 338–349.
- Letnikova, E.F., Geletii, N.K., 2005. Vendian–Cambrian carbonate sequences in the sedimentary cover of the Tuva–Mongolian microcontinent. *Litologiya i Poleznye Iskopaemye*, No. 2, 192–204.
- Lukin, L.I., Chernyshev, V.F., Kushnarev, I.P., 1965. *Microfabric Analysis: A Handbook for Students of Ore Deposits* [in Russian]. Nauka, Moscow.
- Mazukabzov, A.M., Donskaya, T.V., Gladkochub, D.P., Paderin, I.P., 2010. The Late Paleozoic geodynamics of the West Transbaikalian segment of the Central Asian fold belt. *Russian Geology and Geophysics (Geologiya i Geofizika)* 51 (5), 482–491 (615–628).
- Mel'nikov, A.I., Vasil'ev, E.P., Reznitskii, L.Z., Sizykh, A.I., Barash, I.G., 2001. *Methods for the Structural Analysis of Polymetamorphic Complexes* [in Russian]. Internet Engineering, Moscow.
- Obruchev, S.V., 1964. *The Precambrian in the East Sayan* [in Russian]. Nauka, Moscow–Leningrad.
- Passchier, C.W., Trouw, R.A.J., 1996. *Microtectonics*. Springer, Berlin–Heidelberg.
- Reznitskii, L.Z., Sal'nikova, E.B., Barash, I.G., Belichenko, V.G., Glebovitskii, V.A., Kotov, A.B., Kovach, V.P., Yakovleva, S.Z., Fedoseenko, A.M., 2007. Upper age boundary of the accretion of terranes in the northwestern part of the eastern segment of the Central Asian Foldbelt. *Dokl. Earth Sci.* 414 (4), 548–551.
- Rodygin, A.I., 2001. *Dynamically Metamorphosed Rocks* [in Russian]. Izd. Tomsk. Univ., Tomsk.
- Rytsk, E.Yu., Sal'nikova, E.B., Kovach, V.P., Glebovitskii, V.A., Skopintsev, V.G., Kotov, A.B., Gusev, Yu.P., Yakovleva, S.Z., Fedoseenko, A.M., Plotkina, Yu.V., 2000. Upper age boundary of the Oka Group (Eastern Sayan). *Dokl. Earth Sci.* 374 (7), 1080–1083.
- Saranchina, G.M., 1963. *The Fedorov Method*, 2nd ed. [in Russian]. Izd. Leningradsk. Univ., Leningrad.
- Savel'eva, V.B., Travin, A.V., Zyryanov, A.S., 2003. The  $^{40}\text{Ar}$ – $^{39}\text{Ar}$  dating of metasomatic rocks in deep fault zones of the marginal suture of the Siberian Platform. *Dokl. Earth Sci.* 391A (6), 862–865.
- Savel'eva, V.B., Kostitsyn, Yu.A., Travin, A.V., Ponomarchuk, V.A., Moshchenko, A.S., 2006. Geochemistry and Rb–Sr age of graphite-bearing granitoids in the southeast of the Main Sayan Fault. *Russian Geology and Geophysics (Geologiya i Geofizika)* 47 (2), 218–236 (216–231).
- Savel'eva, V.B., Larionov, A.N., Travin, A.V., 2010. Age and geodynamic setting of granitoids in the southeastern Main Sayan Fault, in: *Geodynamic Evolution of the Lithosphere of the Central Asian Mobile Belt (from Ocean to Continent)* (14–17 October 2010, Irkutsk) [in Russian]. IZK SO RAN, Irkutsk, Vol. 2, pp. 64–66.
- Tsygankov, A.A., Matukov, D.I., Berezhnaya, N.G., Larionov, A.N., Posokhov, V.F., Tsyrenov, B.Ts., Khromov, A.A., Sergeev, S.A., 2007. Late Paleozoic granitoids of western Transbaikalia: magma sources and stages of formation. *Russian Geology and Geophysics (Geologiya i Geofizika)* 48 (1), 120–140 (156–180).
- Tsygankov, A.A., Litvinovsky, B.A., Jahn, B.M., Reichow, M.K., Liu, D.Y., Larionov, A.N., Presnyakov, S.L., Lepekhina, Ye.N., Sergeev, S.A., 2010. Sequence of magmatic events in the Late Paleozoic of Transbaikalia, Russia (U–Pb isotope data). *Russian Geology and Geophysics (Geologiya i Geofizika)* 51 (9), 972–994 (1249–1276).
- Turkina, O.M., Nozhkin, A.D., Bayanova, T.B., Dmitrieva, N.V., Travin, A.V., 2007. Precambrian terranes in the southwestern framing of the Siberian craton: isotopic provinces, stages of crustal evolution and accretion–collision events. *Russian Geology and Geophysics (Geologiya i Geofizika)* 48 (1), 61–70 (80–92).
- Turner, F.J., Weiss, L.E., 1963. *Structural Analysis of Metamorphic Tectonites*. McGraw-Hill, New York.
- Twiss, R.J., Moores, E.M., 1992. *Structural Geology*. Freeman, New York.
- Vilor, N.V., Medvedeva, T.I., Bogdanov, G.V., 1991. Endogenic associations of the eastern Tunka Goltsy (East Sayan). *Geologiya i Geofizika (Soviet Geology and Geophysics)* (7), 17–26 (13–20).